Origins of the suppression of fibril formation in grafted methylcellulose solutions

Vaidyanathan Sethuraman and Kevin D. Dorfman*
Department of Chemical Engineering and Materials Science, University of Minnesota—Twin Cities, 421 Washington Ave. SE, Minneapolis, Minnesota 55455, USA

(Received 31 May 2020; accepted 16 July 2020; published 4 August 2020)

We utilize coarse-grained molecular-dynamics simulations to probe the influence of grafting on the conformation and aggregation of methylcellulose chains in water, inspired by the recent experiments on solutions of methylcellulose (MC) chains grafted with polyethylene glycol (PEG) that showed inhibition of methylcellulose fibril formation at high PEG-grafting densities [S. Morozova *et al.*, Macromolecules (Washington, DC, U. S.) **51**, 9413 (2018)]. These simulations reveal three features of the grafted system that should frustrate fibril assembly. First, multichain simulations indicate that the distance between the centers of mass of the chains increases at high grafting densities, suggesting that the ability to form collapsed structures is disrupted. Second, single-chain simulations using grafted MC show that the formation of the precursor toroidal structure responsible for fibril formation is hampered at high grafting densities. Third, the frequency spectrum of conformational fluctuations indicates that low-frequency modes dominate at higher grafting densities, suggesting a larger decorrelation time in conformational fluctuations. Together, these results provide a macromolecular basis for the suppression in fibril formation in grafted methylcellulose solutions for grafting densities exceeding approximately 10%.

DOI: 10.1103/PhysRevMaterials.4.085601

I. INTRODUCTION

Methylcellulose (MC) is a cellulose-based biopolymer [1–6] that undergoes a lower critical solution temperature (LCST) phase transition to form stable hydrogels when heated above 50 °C [1–11]. This thermoreversible gelation property of MC makes it an attractive candidate for applications in, for example, food processing, concrete and pharmaceuticals [8,12,13]. Recent works have gradually revealed the mechanism of gelation in MC solutions [14–17]. In particular, Lodge, Bates and coworkers used cryo-transmission electron micrography in conjunction with small angle neutron scattering (SANS) to show that MC in water forms fibril-like structures [16–19] of constant diameter (14 ± 1 nm) when heated above their LCST [15–17]. In addition, small angle x-ray scattering (SAXS) and SANS studies yielded two notable results: (i) the composition of the fibrils is 60% water and 40% polymer by volume [6,15], and (ii) the fibril diameter is independent of the temperature of formation, molecular weight of MC, and the concentration of the solution [15,16].

The current simulation work is motivated by two recent experiments: (i) Morozova and Lodge [20] used both static and dynamic light scattering to show that the radius of gyration of the polyethylene glycol (PEG) grafted polymer increased with increasing grafting densities. Furthermore, they showed that their results are consistent with theoretical predictions for a grafted chain [21]. They attributed the increase in the radius of gyration to the increased excluded volume repulsion between the backbone MC chains owing to the presence of the grafts [20]. (ii) When the MC backbone is grafted with PEG, Morozova *et al.* [22] observed a systematic suppression of fibril formation with increasing grafting density. Using atomic force microscopy and SAXS on PEG-grafted MC, they showed that there exists a transition from anisotropic fibril-like structures to isotropic structures with increasing number of graft sites per MC chain [22]. They also demonstrated that this transition occurred at lower grafting densities for higher graft molecular weights. However, apart from experimental speculations, the origins of the aforementioned observations remain poorly understood.

It is reasonable to assume that the ability to form a fibril is connected to the morphology of the PEG-grafted MC chains. Several theoretical [21,23–27] and simulation works [28–48] have investigated the influence of grafting on the statics of linear grafted chains. Depending on the grafting density, linear grafted chains can be classified into comb-like chains (low grafting density) or bottlebrush chains (high grafting density) [31,32,49]. Seminal works by Birshtien [23] and Fredrickson [21] showed the influence of steric hindrance on the local structure and rigidity of an isolated chain using scaling theories. Subsequently, Monte Carlo simulations aimed at understanding the lyotropic behavior of bottlebrush chains [41,47] in a dilute athermal solvent showed that the ratio between the persistence length and the bottlebrush diameter is (i) independent of the side-chain length, and (ii) increases with increasing side-chain monomer volume. Effects of side chain rigidity [26,39,40,42,45] and convex graft surfaces were also investigated by using theory [50,51] and simulations [37,38]. Recently, analytical theories and molecular-dynamics simulations [30–32] in the context of grafted copolymers in a melt delineated the influence of grafting on the overlap between chains [31,32,49] and on the mechanical properties [30] of the melt.

A few other simulation studies have focused on quantifying the changes in shape (or conformation) of polymer

*dorfman@umn.edu

 ©2020 American Physical Society

backbone with grafting [36,52,53], but differ in important ways from the grafted MC system considered in this work. For example, simulation studies of flexible comb-copolymers with attractive side-chain interactions showed that, for a long backbone length, side chains form spherical micelles with the backbone wrapped around them [36]. This is somewhat different than the PEG-grafted MC system, which comprises a semiflexible backbone with backbone dihedral interactions and flexible side chains. Furthermore, previous studies [36,52] considered the backbone to be a homopolymer (comprised of one interaction parameter) with excluded volume interactions, whereas in our work, we consider the random copolymer backbone with attractive interactions arising from the different substitutions in MC [1,6]. Finally, while the previous study pertained to understanding the coil-globule phase transition [36], our effort lies in understanding the influence of grafting on the ability to form fibril-like structures.

Motivated by the lack of a thorough understanding of the influence of grafting on fibril formation in MC systems, we use coarse-grained molecular-dynamics simulations to probe the conformational changes in the MC backbone upon grafting and the ability for multiple chains to aggregate in solution. Theory and simulations in the context of bare MC chains have furnished insights into the conformations [54–58], self-assembly mechanisms [55–59], and stability [56,58,60,61] of MC chains in solution. To understand the origins of suppression of fibril formation in grafted MC chains, we revisit the necessary conditions for fibril formation in bare MC chains above the LCST [58]: (i) presence of a precursor toroidal structure, (ii) presence of conformational fluctuations, and (iii) collapse into a continuous fibril-like structure. For the latter, the centers of mass between chains must be be within a minimum capture radius for a bare chain, so that thermal fluctuations enable a growing fibril to engulf a free MC chain.

A plausible hypothesis for the suppression of fibril formation in the experiments of Morozova *et al.* [22] is that the aforementioned conditions for fibril formation are violated in a generic way by grafted MC systems, independent of the particular physicochemical interactions of a MC-PEG system. To this end, we performed coarse-grained simulations of MC chains with flexible side chains. To generalize our observations, we do not specifically examine PEG-grafted MC. Instead, we utilize the model developed by Huang *et al.* [56] for the MC backbone along with flexible grafts and systematically vary the interactions between the backbone and grafts to understand the influence of grafting on MC systems.

II. SIMULATION DETAILS

A. Simulation setup

We employed coarse-grained molecular dynamics to analyze the conformations of PEG-grafted MC in solution. Simulations were performed by using the LAMMPS package [62]. The simulation setup and protocol are similar to our previous work [58]. We focus here on the additions to the previous methodology. For completeness, the rest of the simulation protocol, including the details of the MC model of Huang *et al.* [56], is relegated to Sec. S1 of the Supplemental Material [63].

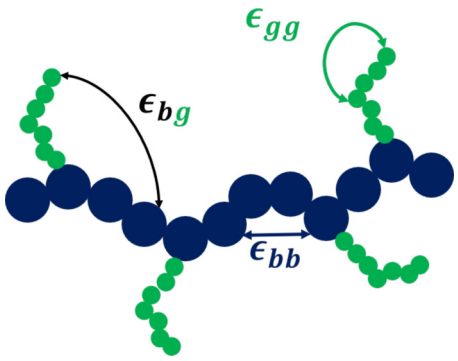

FIG. 1. Schematic of a MC chain (blue) with "PEG-like" graft monomers (green). Nonbonded interaction parameters between graft-graft (ϵ_{gg}), graft-backbone (ϵ_{bg}), and backbone-backbone (ϵ_{bb}) are depicted.

The grafting density Σ is defined as the ratio between the number of graft points per chain to the number of backbone monomers. Σ was varied between 0.01 and 0.3 for all the systems studied. Graft sites along the backbone of the MC chain were chosen at random. The degree of polymerization of the graft (N_g) and the backbone (N_{bb}) were fixed at 25 and 1000, respectively. The ratio between the molecular weights of MC and the grafts are similar to the lower molecular weight graft experiments reported by Morozova *et al.* [20,22].

B. Interaction potentials

Figure 1 displays the schematic of a MC chain (blue) with grafts (green) on its backbone. The bonded and nonbonded interactions for the backbone are adapted from Ref. [56]. The bonded potential U_b between adjacent monomers of a grafted chain as well as that between graft and backbone MC monomer, was modeled by using a harmonic potential of the form

$$U_b = k_b(r-\sigma)^2, \tag{1}$$

where the stretching constant k_b is set to $500k_BT/\sigma^2$.

Nonbonded interactions (U_{nb}) between graft monomers as well as between graft and backbone monomers are modeled by using a 9-6 Lennard-Jones potential of the form

$$U_{nb} = \begin{cases} 4\epsilon_{ij}\left[\left(\frac{\sigma_{ij}}{r}\right)^9 - \left(\frac{\sigma_{ij}}{r}\right)^6\right], & r < r_c \\ 0, & r \geqslant r_c, \end{cases} \tag{2}$$

where ϵ_{ij}, σ_{ij}, and r_c correspond to the nonbonded interaction parameter, average diameter and cutoff for interactions between monomers i and j, respectively. The potential is shifted and cut off at r_c. These nonbonded interactions depend on the type of MC monomer [56,63].

We emphasize that, while the experiments that motivate our analysis were conducted using PEG-grafted MC [20,22], in this work we explore the effects of a "PEG-like" model graft monomers on MC backbone. To this end, we chose three different values {0.8, 1.0, 1.2} for the graft-graft nonbonded interaction parameter ϵ_{gg}. To rationalize the choice of these values, we note that the average interaction parameter between backbone MC monomers (ϵ_{bb}) are between 1.0 and 3.0 in

reduced units [56]. Hence, our range of ϵ_{gg} corresponds to a system where the interactions between graft monomers are weaker than the backbone-backbone interactions. This choice allows us to model a system where there exists a competition between the backbone-backbone attraction and backbone-graft attraction, which leads to interesting behavior. In contrast, if the graft-graft interactions are of similar strength compared with the backbone-backbone interactions ($\epsilon_{gg} \approx \epsilon_{bb}$), the chains collapse owing to the lack of enthalpic penalty from backbone-graft repulsion. If ϵ_{gg} is strongly repulsive compared with ϵ_{bb}, then the time step needed for equilibration becomes very small owing to the presence of strong backbone-graft interactions and the chemical bonding between the backbone and the graft, making this system less robust for simulation.

The backbone-graft interaction parameter ϵ_{bg} is obtained by using the geometric mixing rule $\epsilon_{bg} = \sqrt{\epsilon_{bb}\epsilon_{gg}}$. With increasing ϵ_{gg}, the interaction strength between graft-graft and graft-backbone strengthens. Thus, a graft with $\epsilon_{gg} = 0.8$ is more "repulsive" to the backbone compared with $\epsilon_{gg} = 1.2$.

We note that, instead of varying ϵ_{gg} systematically and deducing ϵ_{bg} using mixing rules, one could instead vary ϵ_{bg} and compute ϵ_{gg}. However, there are eight monomer types for the backbone MC in our simulations. Thus, in the absence of a unique way to vary ϵ_{bg} systematically, it is more straightforward to vary ϵ_{gg}.

Since we are interested in the qualitative changes to the effect of grafting on fibril formation, for ease of calculation, we chose the function for nonbonded potentials identical to that of the MC backbone monomers [Eq. (2)]. In addition, since the graft monomers used in experiments are flexible polymers (as opposed to relatively stiff MC backbone) [22], bonded potentials were modeled as harmonic functions [Eq. (1)], i.e., without the bending and dihedral potentials used for the MC backbone. To obtain a more quantitative comparison for a PEG-grafted system, one must coarse-grain the grafted system (with the graft monomer of interest) to identify the effect of grafts on MC backbone, which is beyond the scope of this work. Using a different coarse-grained model for the graft monomer is also another approach. However, the mixing rules will make the cross interactions in these cases somewhat arbitrary. Given these constraints, to understand a wider range of physical systems (and not their chemical specificity), we chose interaction values based on the heuristics above.

We also need to set the mass and diameter of the graft monomers. We thus chose values that closely mimic PEG such that our model is "PEG-like" even if we have not undertaken a rigorous coarse graining of an atomistic PEG model. The reduced mass of each graft monomer is chosen to be 0.28, which corresponds to the ratio between the average molar mass of a PEG monomer and a MC monomer. The diameter of graft beads are set to be 0.8 times the diameter of a MC bead, which corresponds approximately to the ratio between the size of a PEG monomer and that of a MC monomer. The cutoff radius was also set to 0.8 times the average cutoff radii of all MC monomer types. For completeness, all the interaction parameters along with their variation as a function of distance r are tabulated in Table S1 and Fig. S1 of the Supplemental Material [63].

C. Quantification measures: Shape factor

The shape anisotropy factor κ_i^2 of a polymer chain [64] is computed from the eigenvalues of its radius of gyration tensor by using

$$\kappa_i^2 = \frac{3\left(\lambda_x^4 + \lambda_y^4 + \lambda_z^4\right)}{2\left(\lambda_x^2 + \lambda_y^2 + \lambda_z^2\right)^2} - \frac{1}{2}, \tag{3}$$

where λ_x^2, λ_y^2, and λ_z^2 are the eigenvalues of the radius of gyration tensor of the polymer backbone (excluding grafts). The values of $\kappa_i^2 = 0$, 0.25, and 1.0 correspond to a straight line, ring, and sphere, respectively. Our previous works [58,59] showed that the change in shape anisotropy factor is a convenient measure to quantify conformational fluctuations.

For brevity, we relegate to Sec. S2 of the Supplemental Material [63] other definitions for the more common conformational measures such as the square of the radius of gyration $\langle R_g^2 \rangle$ and the distance between the centers of mass d_{COM}, along with the Fourier transform of shape anisotropy factor and error quantification.

Results from four independent initial configurations are averaged and reported.

III. RESULTS

A. Ability to form fibrils

Our previous work on bare chains (i.e., an ungrafted system) showed that the chains need to be present within a minimum capture radius ($\simeq 20\sigma$) to form a protofibril structure [58] through diffusion and conformational fluctuations. To probe the influence of grafting on the ability of the MC chains to form a protofibril structure over a similar timescale as we observed for ungrafted MC, we perform two-chain simulations with grafts such that the initial distance between the centers of mass (d_{COM}) of the chains (including the grafts) is approximately equal to 20σ.

Figure 2(a) displays the ensemble averaged normalized mean distance between the centers of mass $\langle d^*_{\mathrm{COM}} \rangle$ [Eq. (S4)] of two chains as a function of grafting density for three different interaction parameters. When the attraction between the graft and the backbone is strongest ($\epsilon_{gg} = 1.2$), irrespective of the grafting density, the normalized final distance of approach between the chains was similar to that of a bare chain (green circles). This result suggests that the chains will collapse onto each other at high grafting densities for strong graft-backbone attraction, but does not necessarily imply that the final structure is the same protofibril observed for bare chains.

Furthermore, with increasing repulsion between the grafts and the backbone ($\epsilon_{gg} = \{0.8, 1.0\}$) and at low grafting densities ($\Sigma \leqslant 0.1$), the equilibrium distance between the centers of mass is approximately equal to that of a bare chain. Hence, at low grafting densities, irrespective of the interactions between the grafts, fibril formation should not be disrupted. However, beyond a critical grafting density ($\Sigma \approx 0.15$), the distance between the centers of mass steadily increases with increasing grafting density, suggesting that the chain collapse will be disrupted at high grafting densities for these interaction strengths.

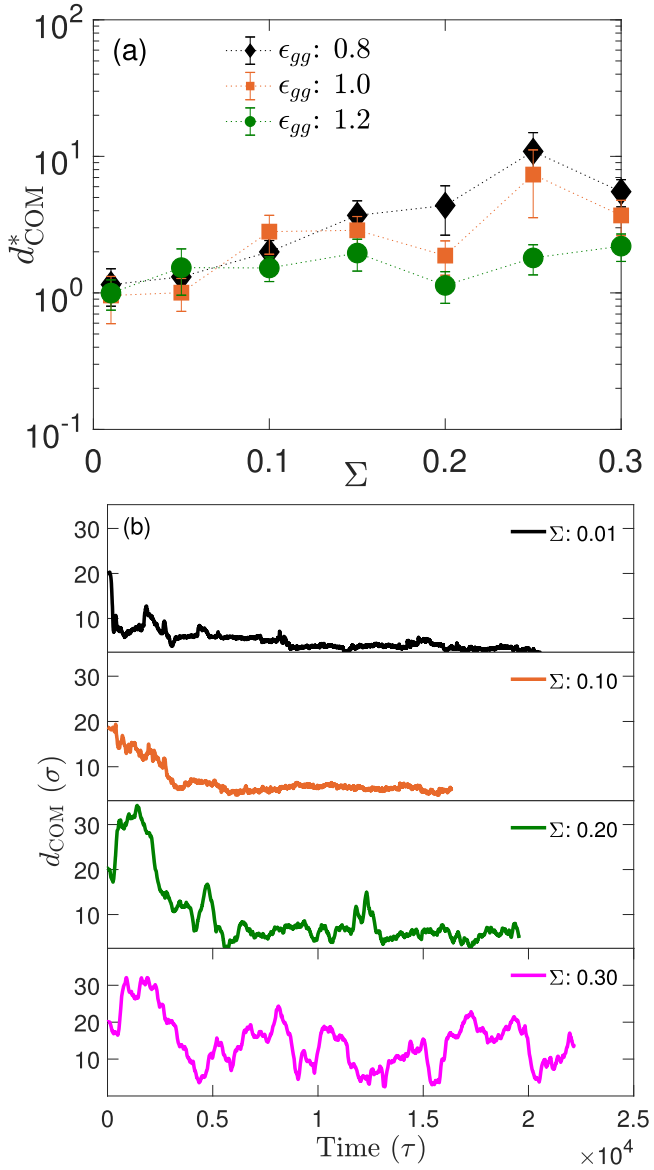

FIG. 2. (a) Normalized distance between the centers of mass computed by using the positions of both the backbone monomers and graft monomers for two-chain systems as function of grafting density for different graft-graft interactions. The corresponding distance between the centers of mass for a bare MC system ($\Sigma = 0$) is $3.61 \pm 0.59\sigma$. (b) The distance between centers of mass for two-chain systems as a function of time for various grafting densities at $\epsilon_{gg} = 0.8$.

To explore the chain dynamics in more detail, the time evolution of the distance between the centers of mass of the two chains d_{COM} is shown for a set of grafting densities in Fig. 2(b) for the strongest repulsion between the grafts and backbone ($\epsilon_{gg} = 0.8$). At low grafting densities, the chains collapse onto each other within 5000τ, as evidenced by the small distance between the centers of mass of the two chains ($\leqslant 3.0\sigma$). However, at higher grafting densities, the distance between the centers of mass do not converge, suggesting that the chains do not collapse. This result is indeed consistent with the average d^*_{COM} in Fig. 2(a). Furthermore, this result

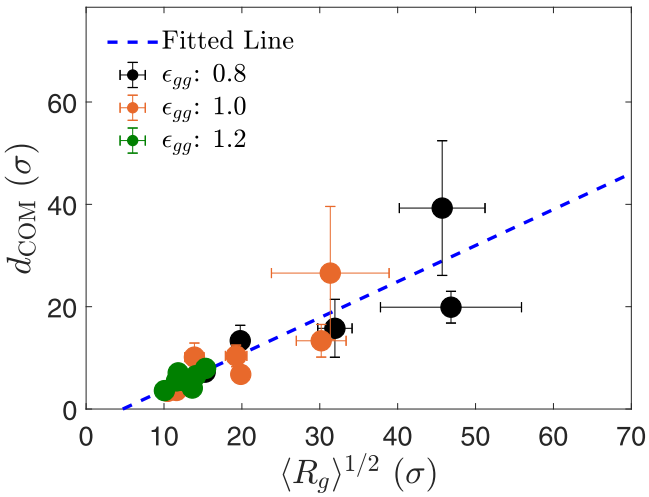

FIG. 3. Distance between the centers of mass for two-chain systems as a function of the average radius of gyration of the system. Dashed line shows the best-fit line.

shows that the timescale for collapse gradually increases with increased graft density until the chains can no longer collapse at $\Sigma = 0.3$.

To test whether the average radius of gyration, $\langle R_g^2 \rangle^{1/2}$, is the length scale controlling the steric hindrance leading to the disruption in the collapse of the chains, we plot the ensemble averaged distance between the centers of the chains d_{COM} as a function of $\langle R_g^2 \rangle^{1/2}$ in Fig. 3. The data at low grafting densities collapse nicely onto the best-fit line (blue dashed line) whereas the data begin to deviate slightly at high grafting densities. This result suggests that, while $\langle R_g^2 \rangle^{1/2}$ is indeed one of the key length scales governing the equilibrium distance of approach, other length scales play a role in determining the equilibrium distance of approach at high grafting densities.

B. Nucleating structure

Previous experimental [16–18] and simulation works [55,58,59] have suggested a nucleation and growth type mechanism for fibril formation in bare MC chains. Furthermore, simulation works [55,58,59] showed that a toroidal nucleating structure is essential for fibril formation in bare MC chains. To understand the influence of grafting on the nucleating structure, we analyze the conformations of isolated MC chains with grafts.

Figure 4 displays the $\langle R_g^2 \rangle$ of an isolated MC chain (computed such that it includes the side chains) normalized with the square of the radius of gyration of the bare chain $\langle R_{g0}^2 \rangle$ as a function of the grafting density Σ, for three different backbone-graft interactions (ϵ_{gg}). At low grafting densities ($\Sigma \leqslant 0.1$), $\langle R_g^2 \rangle$ is a constant irrespective of the backbone-graft interactions. When the interaction between grafts and backbone is strongly repulsive ($\epsilon_{gg} = 0.8$), $\langle R_g^2 \rangle$ increases with increasing grafting density. In contrast, when the interactions between the graft and backbone become less repulsive ($\epsilon_{gg} = 1.2$), $\langle R_g^2 \rangle$ becomes independent of the grafting density.

Figure 5(a) displays the effects of the interaction parameters and the grafting densities on the equilibrium conformation of the nucleating structure in terms of a "phase diagram";

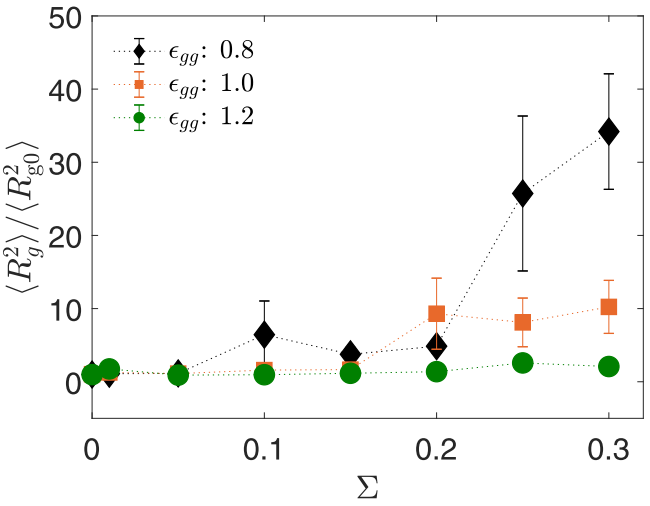

FIG. 4. Square of the radius of gyration of the chain (computed using both the backbone and the grafts) normalized with bare radius of gyration (no grafts) as a function of the grafting density for different backbone-graft interactions. The calculated value of the square of the bare radius of gyration ($\langle R_{g0}^2\rangle$) is $87.72 \pm 6.47\sigma^2$. $\langle R_g^2\rangle$ values obtained from individual runs are tabulated in Tables S2 and S3 of the Supplemental Material [63].

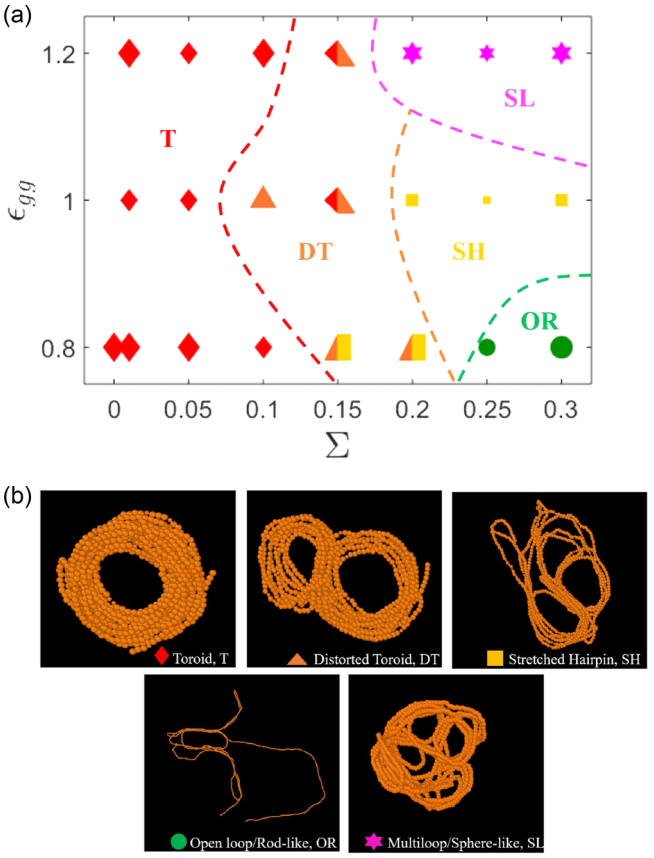

FIG. 5. (a) Phase diagram of the grafted methylcellulose system, where the acronyms refer to the structures in panel (b). If two structures are equally likely, legends of the conformations are fused and shown. Results from all independent runs, along with their frequency of occurrence, are tabulated in Table S4. Marker sizes correspond to the probability of finding that given configuration. Phase boundaries depicted by using dashed lines are a guide for the eye; (b) Snapshots depicting various single-chain configurations. The legend at the bottom of each snapshot displays the name given to the shape at equilibrium, and the acronym corresponds to the key in panel (a). Only the backbone chain is represented for clarity. Figures are rendered using OVITO software [65].

we use quotation marks here to emphasize that the structures we observe are likely kinetically trapped. The most probable configuration from at least four different initial configurations are reported in Fig. 5(a). Marker sizes correspond to the probability of occurrence for a given configuration. At equilibrium, chains undergo instantaneous conformational fluctuations but relax (on an average) to structures similar to those shown in Fig. 5(b). Near "phase-transition" boundaries, owing to kinetic traps, the configurations that straddle the boundary may be equally likely (metastable structures). For these tied cases, legends of the corresponding conformations are fused and shown. For instance, the marker representing some of the points near the toroid-distorted toroid transition ($\{\Sigma = 0.15,\ \epsilon_{gg} = 1.0\}$ and $\{\Sigma = 0.15,\ \epsilon_{gg} = 1.2\}$) consist of both red diamonds (for toroids) and orange triangles (distorted toroids). Since we have identified only four different realizations of any given point, the conformation of the polymer chain near these points cannot be determined with absolute certainty. Furthermore, we note that the loci of the phase boundary are approximate and should be taken as guidelines for the eye. Results from all independent runs, along with their frequency of occurrence, are tabulated in Table S4 of the Supplemental Material [63].

For $\Sigma = 0$ (ungrafted chains), the randomly coiled chains relax to form toroidal structures and their conformations are consistent with the previous work [58]. By definition, these results do not depend upon the interaction between the graft and the backbone. For convenience, we display this at the (x, y) coordinate $(\Sigma = 0, \epsilon_{gg} = 0.8)$.

At low grafting densities ($\sigma \lessapprox 0.1$), irrespective of the interaction strength between the backbone and graft monomers, single-chain methylcellulose retains its toroidal nucleating structure. These results suggest that the ability to form fibril-like structures should be retained at low grafting densities and are consistent with experiments [22]. An isolated grafted methylcellulose chain forms a toroidal structure or a distorted toroidal structure at intermediate grafting densities ($0.1 \lessapprox \Sigma \lessapprox 0.2$). The probability to form these structures depends on the interaction strength between the backbone and the graft.

At higher grafting densities ($\Sigma \gtrapprox 0.2$), a stretched-hairpin structure is obtained for $\epsilon_{gg} = 1.0$. These structures are also observed at a lower grafting density ($0.1 \lessapprox \Sigma \lessapprox 0.2$) when $\epsilon_{gg} = 0.8$. For $\epsilon_{gg} = 0.8$ and 1.0, near the "phase-boundaries," the structures obtained were metastable and are evinced by the almost equal frequency of occurrence for multiple possible structures (cf. Table S4 of the Supplemental Material [63]). Figure S2 of the Supplemental Material [63] shows the final configurations for this region of the phase space.

For $\Sigma \gtrapprox 0.2$ and $\epsilon_{gg} = 0.8$, open-loop or rod-like structures are observed. When the graft-backbone interaction strength becomes more attractive, the final configuration assumes a stretched hairpin structure at intermediate

backbone-graft interactions ($\epsilon_{gg} = 1.0$) and a sphere-like structure when the backbone-graft interactions is strongly attractive ($\epsilon_{gg} = 1.2$).

We note that a nonmonotonic trend is observed in the phase diagram at intermediate grafting densities ($\Sigma \approx 0.1$) and at intermediate interaction strengths ($\epsilon_{gg} = 1.0$). However, this may be a simulation artifact arising from the lack of sampling of the structures in this region. Further independent simulations need to be performed to identify whether this trend arises from simulation artifacts and can be taken up as a future work.

C. Conformational fluctuations

To understand the influence of grafting on the conformational fluctuations that enable the nucleating toroid to engulf a neighboring chain, we compute the shape factor [Eq. (3)] and temporal changes in the shape factor. To quantify the conformational fluctuations we explicitly examine (i) the changes in the magnitude of κ^2 as a function of time, $|d\kappa^2/dt|$, and (ii) the fundamental modes of κ^2. We examine the real-time spectrum of κ^2 for the former and the Fourier spectrum for the latter.

Figure 6(a) displays the shape factor as a function of time for different grafting densities with $\epsilon_{gg} = 0.8$, for one of the four independent simulations. Qualitatively similar results are obtained for the other three simulations (cf. Fig. S3). The top panel of Fig. 6(a) shows the time evolution of κ^2 for the lowest grafting density studied ($\Sigma = 0.01$) and is similar to the bare-chain results [58]. Both the value of the shape factor and its fluctuation frequency change with increasing grafting density. Comparing with low grafting densities ($\Sigma \leqslant 0.1$), at higher grafting densities ($\Sigma \geqslant 0.2$) the magnitude of the change in the values of κ^2 with respect to time, $|d\kappa^2/dt|$, is much larger.

To quantify this smoothness (or the presence of different fundamental modes of κ^2), Fig. 6(b) displays representative data for the fluctuation modes as a function of the fundamental frequencies $\omega/(2\pi)$. The corresponding real-time κ^2 data are shown in the inset of Fig. 6(b). A smoother variation in the real-time data for κ^2 qualitatively indicates that the long-wavelength modes are dominant relative to the short-wavelength modes. For higher grafting densities, $\kappa^2(\omega)$ for small ω [$\omega/(2\pi) \lessapprox 10^{-3}\tau^{-1}$] is at least an order of magnitude higher for systems with higher grafting densities, showing that the low-frequency modes are significantly larger at higher grafting densities. Together, the results in this section show that, while the changes in the magnitude of κ^2 are larger at high grafting densities ($\Sigma \geqslant 0.2$), long-wavelength modes are dominant relative to the short-wavelength modes for the fluctuations in κ^2.

IV. DISCUSSION

Results in the previous section unequivocally showed that there exists a suppression of the conditions deemed necessary for fibril formation in grafted methylcellulose solutions at high grafting densities. In this section, we provide energetic arguments to explain the results at both low and high grafting densities, and interpret our results in the context of what we would anticipate to happen to fibril formation in a many-chain system based on the one-chain and two-chain systems.

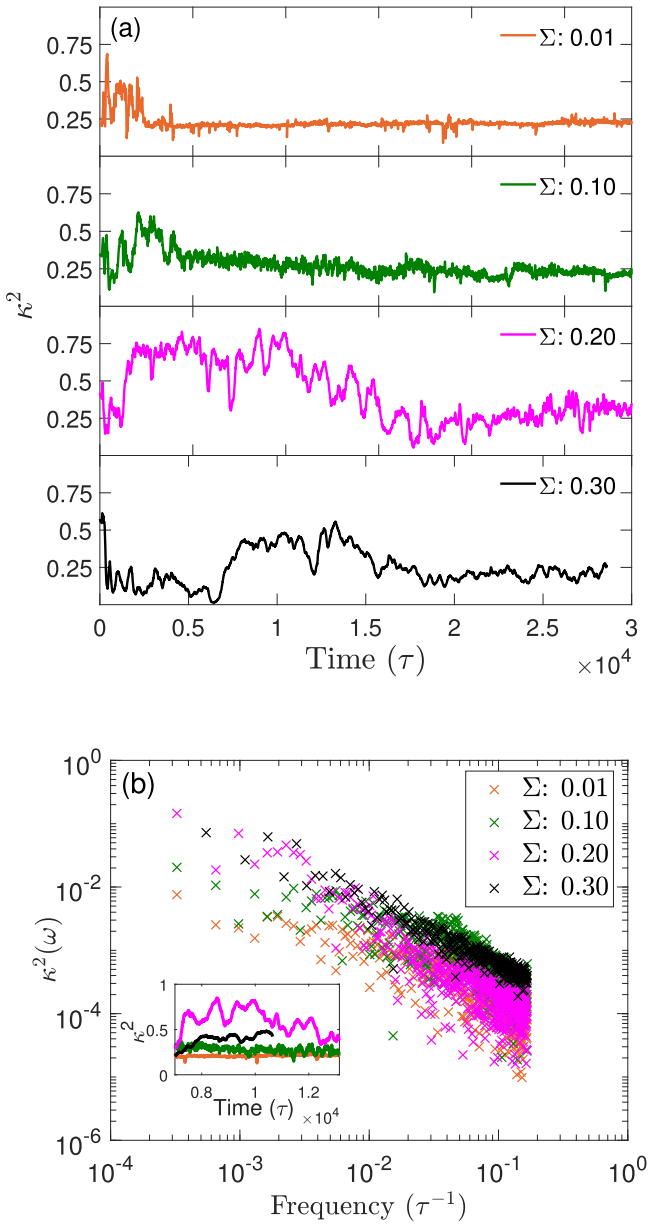

FIG. 6. (a) Shape factor as a function of time for different grafting densities with $\epsilon_{gg} = 0.8$. (b) Fourier transform of the shape factor for a subset of the data given in panel (a). The data in panel (a) used to obtain the frequency spectra are plotted in the inset. Additional figures depicting the shape factor for other initial conditions and the Fourier transform of the shape factor are displayed in Figs. S3 and S4 of the Supplemental Material [63].

At low grafting densities ($\Sigma \lessapprox 0.1$), owing to the smaller number of grafts and the side chain's molecular weight (in comparison to backbone molecular weight), the enthalpic and entropic contributions to the free energy from the backbone-graft interactions are minimal, irrespective of the graft-backbone interactions studied. For these cases, the conformational properties of the single-chain grafted systems (Figs. 4–6) are primarily determined by a competition between the backbone-backbone dihedral interactions, which favor a planar structure, and the self-attractive backbone-backbone interactions, similar to the competition governing

the conformations of ungrafted chains [58]. Furthermore, the changes in $\kappa^2(\omega)$ [Fig. 6(b)] over the entire frequency spectrum are small compared with those at higher grafting densities, suggesting the presence of stronger high-frequency fluctuations, or equivalently a shorter decorrelation time in κ^2. Again, this behavior resembles that observed in ungrafted chains [58,59]. In multichain systems, the steric hindrances arising from the presence of grafts are weak, leading to the collapse of multiple chains (Fig. 2). These observations are consistent with fibril formation being retained at low grafting densities, since the structure and dynamics of the grafted system are effectively unchanged up to a grafting density of 10%.

A transition zone is observed at intermediate grafting densities ($0.1 \lessapprox \Sigma \lessapprox 0.2$), wherein the conformational properties of the grafted MC chains begin to deviate from those of the ungrafted MC chains [58]. Furthermore, the magnitude of deviation increases with increasing repulsion between the graft and the backbone, or equivalently, decreasing ϵ_{gg}. It is unclear, based on our models [58] for extrapolating the physics of single MC chains and two-chain systems to fibril formation, whether these deviations are sufficient to suppress fibril formation in experiments.

The deviations from the ungrafted and the low graft density cases arise from a competition between two effects: On the one hand, the grafts are attractive and hence grafts tend to be near each other to minimize enthalpy. On the other hand, for multichain systems, the entropic cost arising from steric hindrance becomes stronger with increasing grafting densities, thereby pushing the chains away. In addition, at high grafting densities with strong backbone-graft repulsion ($\epsilon_{gg} = \{0.8, 1.0\}$), when the chains are close to each other, grafts in a given chain experience strong backbone repulsion from both their parent chain and from other chains, thereby contributing to the steric hindrance. These competing effects also explain the presence of a local maximum in d_{COM} [Fig. 2(a)] around $\Sigma = 0.25$ when the backbone-graft interactions are strongly repulsive. For single-chain systems, the backbone-graft repulsion results in the stretching of the backbone leading to an increase in R_g^2 (Fig. 4) and distortion in the toroidal structure (Fig. 5).

For intermediate grafting densities and strong attractive interactions ($\epsilon_{gg} = 1.2$), the conformational properties of the grafted systems do not deviate significantly from those of the ungrafted systems [58]. For these cases, we speculate that the steric hindrance arising from the grafts, which tends to swell the chain, are offset by the graft-graft and the graft-backbone attractions that tend to collapse the chain.

At high grafting densities ($\Sigma \gtrapprox 0.2$), the conformational properties of grafted MC chains (Figs. 2–6) deviate significantly from those of the ungrafted MC chains. For isolated MC chains and at $\epsilon_{gg} = \{0.8, 1.0\}$, the backbone strongly stretches to minimize the backbone-graft contacts. This leads to an approximately sixfold increase in its radius of gyration (Fig. 4) and is consistent with the open-loop and rod-like structures observed in Fig. 5. Furthermore, the ratio between high- and low-frequency modes is larger compared with low grafting densities [Fig. 6(b)], suggesting that the decorrelation time in κ^2 is higher. The presence of weak, slow modes may also contribute to the disruption of fibril formation at higher grafting densities. These low-frequency modes indicate that the nucleating structures at higher grafting densities undergo conformational changes over a much longer timescale compared with lower grafting densities, suggesting that the nucleating structures are metastable. This can be visually corroborated from Fig. 6(a) which shows that κ^2 relaxes slowly to its equilibrium values at higher grafting densities. Thus, the condition of a stable nucleating structure for fibril formation becomes less obvious at higher grafting densities. For multichain systems, the steric repulsion arising from the grafts and strong backbone-graft repulsion result in the disruption of chain collapse.

However, when the backbone-graft interactions are strongly attractive ($\epsilon_{gg} = 1.2$), at a high grafting density, backbone-graft interactions dominate the steric hindrance associated by the larger number of grafts, leading to a collapsed structure (Fig. 2). For isolated MC systems, these attractive graft-backbone interactions lead to a globule-like structure (Fig. 5). These results correspond to the behavior of polymer in a poor solvent and were also observed in previous works on grafted chains with attractive backbone interactions [36]. We speculate that, if there is a disruption in fibril formation under these conditions, it would arise from the disruption of the nucleating structure (cf. Sec. III B) rather than from the inability to form collapsed fibril-like structures [Fig. 2(a)]. Nevertheless, there are no existing experimental results to test this speculation, and we would require many-chain simulations to draw a definitive conclusion about these dynamics from our model.

V. CONCLUSIONS

Motivated by recent experimental findings that fibril formation is suppressed in PEG-grafted methylcellulose solutions at high grafting densities [22], we used coarse-grained molecular-dynamics simulations to understand its origins. Our simulations showed that the nucleating structure forming the fibrils is disrupted at high grafting densities, irrespective of the interactions between the graft and the backbone. Furthermore, we demonstrated that the decorrelation time of the shape anisotropy factor for repulsive graft-graft (or equivalently graft-backbone) interactions increases with increasing grafting densities. Finally, we showed that the equilibrium distance of approach steadily increases with increasing grafting densities when the graft-backbone interactions are strongly repulsive. Together, these simulation results provide a fundamental understanding of the origins of suppression of fibril formation in grafted methylcellulose solutions at high grafting densities.

Code Repository: LAMMPS codes used to generate the trajectories, PYTHON codes used to run the simulations, and FORTRAN codes used to analyze the trajectories can be found in Ref. [66]. Data corresponding to each figure can be found in Ref. [67].

ACKNOWLEDGMENTS

We acknowledge fruitful discussion with Prof. T. P. Lodge (University of Minnesota) and Prof. S. Morozova (Case Western Reserve University). This work was supported primarily by the National Science Foundation through the

University of Minnesota Materials Science Research and Engineering Center under Awards No. DMR-1420013 and No. DMR-2011401. The authors acknowledge the Minnesota Supercomputing Institute (MSI) at the University of Minnesota for providing resources that contributed to the research results reported within this paper.

[1] W. S. Denham and H. Woodhouse, CLXXXVI.–The methylation of cellulose, J. Chem. Soc., Trans. **103**, 1735 (1913).

[2] L. Rebenfeld and E. Pacsu, Cellulose studies: Part XIX. Distribution of methoxyl groups in partly methylated celluloses, Text. Res. J. **24**, 941 (1954).

[3] K. Nishinari, K. E. Hofmann, H. Moritaka, K. Kohyama, and N. Nishinari, Gel-sol transition of methylcellulose, Macromol. Chem. Phys. **198**, 1217 (2003).

[4] E. Heymann, Studies on sol-gel transformations. I. The inverse sol-gel transformation of methylcellulose in water, Trans. Faraday Soc. **31**, 846 (1935).

[5] P. Nasatto, F. Pignon, J. Silveira, M. Duarte, M. Noseda, and M. Rinaudo, Methylcellulose, a cellulose derivative with original physical properties and extended applications, Polymers (Basel, Switz.) **7**, 777 (2015).

[6] S. Morozova, Methylcellulose fibrils: A mini review, Polym. Int. **69**, 125 (2020).

[7] T. Kato, M. Yokoyama, and A. Takahashi, Melting temperatures of thermally reversible gels IV. Methyl cellulose-water gels, Colloid Polym. Sci. **256**, 15 (1978).

[8] T. Ito, Y. Ishikawa, S. Okano, T. Hattori, R. Fujii, T. Shinozawa, and A. Shibuya, Cloning of human neuroblastoma cells in methylcellulose culture, Cancer Res. **47**, 4146 (1987).

[9] P. Colombo, Swelling-controlled release in hydrogel matrices for oral route, Adv. Drug Delivery Rev. **11**, 37 (1993).

[10] V. H. Freedman and S. Shin, Cellular tumorigenicity in nude mice: Correlation with cell growth in semi-solid medium, Cell (Cambridge, MA, U. S.) **3**, 355 (1974).

[11] K. R. Kamath and K. Park, Biodegradable hydrogels in drug delivery, Adv. Drug Delivery Rev. **11**, 59 (1993).

[12] D. Saha and S. Bhattacharya, Hydrocolloids as thickening and gelling agents in food: A critical review, J. Food Sci. Technol. (New Delhi, India) **47**, 587 (2010).

[13] R. Priya, R. Singhal, and P. Kulkarni, Carboxymethylcellulose and hydroxypropylmethylcellulose as additives in reduction of oil content in batter based deep-fat fried boondis, Carbohydr. Polym. **29**, 333 (1996).

[14] J. P. A. Fairclough, H. Yu, O. Kelly, A. J. Ryan, R. L. Sammler, and M. Radler, Interplay between gelation and phase separation in aqueous solutions of methylcellulose and hydroxypropylmethylcellulose, Langmuir **28**, 10551 (2012).

[15] J. R. Lott, J. W. McAllister, M. Wasbrough, R. L. Sammler, F. S. Bates, and T. P. Lodge, Fibrillar structure in aqueous methylcellulose solutions and gels, Macromolecules (Washington, DC, U. S.) **46**, 9760 (2013).

[16] J. W. McAllister, J. R. Lott, P. W. Schmidt, R. L. Sammler, F. S. Bates, and T. P. Lodge, Linear and nonlinear rheological behavior of fibrillar methylcellulose hydrogels, ACS Macro Lett. **4**, 538 (2015).

[17] J. W. McAllister, P. W. Schmidt, K. D. Dorfman, T. P. Lodge, and F. S. Bates, Thermodynamics of aqueous methylcellulose solutions, Macromolecules (Washington, DC, U. S.) **48**, 7205 (2015).

[18] P. W. Schmidt, S. Morozova, S. P. Ertem, M. L. Coughlin, I. Davidovich, Y. Talmon, T. M. Reineke, F. S. Bates, and T. P. Lodge, Internal structure of methylcellulose fibrils, Macromolecules (Washington, DC, U. S.) **53**, 398 (2020).

[19] P. Schmidt, S. Morozova, P. M. Owens, R. Adden, Y. Li, F. S. Bates, and T. P. Lodge, Molecular weight dependence of methylcellulose fibrillar networks, Macromolecules (Washington, DC, U. S.) **51**, 7767 (2018).

[20] S. Morozova and T. P. Lodge, Conformation of methylcellulose as a function of poly(ethylene glycol) graft density, ACS Macro Lett. **6**, 1274 (2017).

[21] G. H. Fredrickson, Surfactant-induced lyotropic behavior of flexible polymer solutions, Macromolecules (Washington, DC, U. S.) **26**, 2825 (1993).

[22] S. Morozova, P. W. Schmidt, F. S. Bates, and T. P. Lodge, Effect of poly(ethylene glycol) grafting density on methylcellulose fibril formation, Macromolecules (Washington, DC, U. S.) **51**, 9413 (2018).

[23] T. M. Birshtein, O. V. Borisov, Y. B. Zhulina, A. R. Khokhlov, and T. A. Yurasova, Conformations of comb-like macromolecules, Polym. Sci. U.S.S.R. **29**, 1293 (1987).

[24] E. B. Zhulina and T. A. Vilgis, Scaling theory of planar brushes formed by branched polymers, Macromolecules (Washington, DC, U. S.) **28**, 1008 (1995).

[25] N. A. Denesyuk, Conformational properties of bottle-brush polymers, Phys. Rev. E **67**, 051803 (2003).

[26] A. Subbotin, M. Saariaho, R. Stepanyan, O. Ikkala, and G. ten Brinke, Cylindrical brushes of comb copolymer molecules containing rigid side chains, Macromolecules (Washington, DC, U. S.) **33**, 6168 (2000).

[27] L. Feuz, F. A. M. Leermakers, M. Textor, and O. Borisov, Bending rigidity and induced persistence length of molecular bottle brushes: A self-consistent-field theory, Macromolecules (Washington, DC, U. S.) **38**, 8891 (2005).

[28] S. Rathgeber, T. Pakula, A. Wilk, K. Matyjaszewski, and K. L. Beers, On the shape of bottle-brush macromolecules: Systematic variation of architectural parameters, J. Chem. Phys. **122**, 124904 (2005).

[29] D. Chatterjee and T. A. Vilgis, Scaling laws of bottle-brush polymers in dilute solutions, Macromol. Theory Simul. **25**, 518 (2016).

[30] Z. Cao, J.-M. Y. Carrillo, S. S. Sheiko, and A. V. Dobrynin, Computer simulations of bottle brushes: From melts to soft networks, Macromolecules (Washington, DC, U. S.) **48**, 5006 (2015).

[31] J. Paturej, S. S. Sheiko, S. Panyukov, and M. Rubinstein, Molecular structure of bottlebrush polymers in melts, Sci. Adv. **2**, e1601478 (2016).

[32] H. Liang, Z. Cao, Z. Wang, S. S. Sheiko, and A. V. Dobrynin, Combs and bottlebrushes in a melt, Macromolecules (Washington, DC, U. S.) **50**, 3430 (2017).
[33] S. Rathgeber, T. Pakula, A. Wilk, K. Matyjaszewski, H.-i. Lee, and K. L. Beers, Bottle-brush macromolecules in solution: Comparison between results obtained from scattering experiments and computer simulations, Polymer **47**, 7318 (2006).
[34] S. Dutta, M. A. Wade, D. J. Walsh, D. Guironnet, S. A. Rogers, and C. E. Sing, Dilute solution structure of bottlebrush polymers, Soft Matter **15**, 2928 (2019).
[35] S. Elli, F. Ganazzoli, E. G. Timoshenko, Y. A. Kuznetsov, and R. Connolly, Size and persistence length of molecular bottlebrushes by Monte Carlo simulations, J. Chem. Phys. **120**, 6257 (2004).
[36] V. V. Vasilevskaya, A. A. Klochkov, P. G. Khalatur, A. R. Khokhlov, and G. ten Brinke, Microphase separation within a comb copolymer with attractive side chains: A computer simulation study, Macromol. Theory Simul. **10**, 389 (2001).
[37] M. Murat and G. S. Grest, Polymers end-grafted onto a cylindrical surface, Macromolecules (Washington, DC, U. S.) **24**, 704 (1991).
[38] E. M. Sevick, Shear swelling of polymer brushes grafted onto convex and concave surfaces, Macromolecules (Washington, DC, U. S.) **29**, 6952 (1996).
[39] Y. Rouault and O. V. Borisov, Comb-branched polymers: Monte Carlo simulation and scaling, Macromolecules (Washington, DC, U. S.) **29**, 2605 (1996).
[40] H.-P. Hsu, W. Paul, and K. Binder, One- and two-component bottle-brush polymers: Simulations compared to theoretical predictions, Macromol. Theory Simul. **16**, 660 (2007).
[41] M. Saariaho, I. Szleifer, O. Ikkala, and G. ten Brinke, Extended conformations of isolated molecular bottle-brushes: Influence of side-chain topology, Macromol. Theory Simul. **7**, 211 (1998).
[42] A. Yethiraj, A Monte Carlo simulation study of branched polymers, J. Chem. Phys. **125**, 204901 (2006).
[43] R. Connolly, G. Bellesia, E. G. Timoshenko, Y. A. Kuznetsov, S. Elli, and F. Ganazzoli, ''Intrinsic" and "topological" stiffness in branched polymers, Macromolecules (Washington, DC, U. S.) **38**, 5288 (2005).
[44] H.-P. Hsu, W. Paul, S. Rathgeber, and K. Binder, Characteristic length scales and radial monomer density profiles of molecular bottle-brushes: Simulation and experiment, Macromolecules (Washington, DC, U. S.) **43**, 1592 (2010).
[45] M. Saariaho, A. Subbotin, I. Szleifer, O. Ikkala, and G. ten Brinke, Effect of side chain rigidity on the elasticity of comb copolymer cylindrical brushes: a Monte Carlo simulation study, Macromolecules (Washington, DC, U. S.) **32**, 4439 (1999).
[46] K. Binder, H.-P. Hsu, and W. Paul, Understanding the stiffness of macromolecules: From linear chains to bottle-brushes, Eur. Phys. J. Spec. Top. **225**, 1663 (2016).
[47] M. Saariaho, O. Ikkala, I. Szleifer, I. Erukhimovich, and G. ten Brinke, On lyotropic behavior of molecular bottle-brushes: A Monte Carlo computer simulation study, J. Chem. Phys. **107**, 3267 (1997).
[48] M. Saariaho, A. Subbotin, O. Ikkala, and G. ten Brinke, Comb copolymer cylindrical brushes containing semiflexible side chains: A Monte Carlo study, Macromol. Rapid Commun. **21**, 110 (2000).
[49] H. Liang, B. J. Morgan, G. Xie, M. R. Martinez, E. B. Zhulina, K. Matyjaszewski, S. S. Sheiko, and A. V. Dobrynin, Universality of the entanglement plateau modulus of comb and bottlebrush polymer melts, Macromolecules (Washington, DC, U. S.) **51**, 10028 (2018).
[50] N. Dan and M. Tirrell, Polymers tethered to curved interfaces: A self-consistent-field analysis, Macromolecules (Washington, DC, U. S.) **25**, 2890 (1992).
[51] R. C. Ball, J. F. Marko, S. T. Milner, and T. A. Witten, Polymers grafted to a convex surface, Macromolecules (Washington, DC, U. S.) **24**, 693 (1991).
[52] Y. Rouault, From comb polymers to polysoaps: A Monte Carlo attempt, Macromol. Theory Simul. **7**, 359 (1998).
[53] A. Gauger and T. Pakula, Static properties of noninteracting comb polymers in dense and dilute media. A Monte Carlo study, Macromolecules (Washington, DC, U. S.) **28**, 190 (1995).
[54] M. Kong, I. Saha Dalal, G. Li, and R. G. Larson, Systematic coarse-graining of the dynamics of self-attractive semiflexible polymers, Macromolecules (Washington, DC, U. S.) **47**, 1494 (2014).
[55] V. V. Ginzburg, R. L. Sammler, W. Huang, and R. G. Larson, Anisotropic self-assembly and gelation in aqueous methylcellulose—theory and modeling, J. Polym. Sci., Part B: Polym. Phys. **54**, 1624 (2016).
[56] W. Huang, R. Ramesh, P. K. Jha, and R. G. Larson, A systematic coarse-grained model for methylcellulose polymers: Spontaneous ring formation at elevated temperature, Macromolecules (Washington, DC, U. S.) **49**, 1490 (2016).
[57] W. Huang, M. Huang, Q. Lei, and R. G. Larson, A simple analytical model for predicting the collapsed state of self-attractive semiflexible polymers, Polymers (Basel, Switz.) **8**, 264 (2016).
[58] V. Sethuraman and K. D. Dorfman, Simulating precursor steps for fibril formation in methylcellulose solutions, Phys. Rev. Materials **3**, 055601 (2019).
[59] X. Li, F. S. Bates, and K. D. Dorfman, Rapid conformational fluctuations in a model of methylcellulose, Phys. Rev. Materials **1**, 025604 (2017).
[60] G. M. Grason, Defects in crystalline packings of twisted filament bundles. I. Continuum theory of disclinations, Phys. Rev. E **85**, 031603 (2012).
[61] M. Jaspers, A. C. H. Pape, I. K. Voets, A. E. Rowan, G. Portale, and P. H. J. Kouwer, Bundle formation in biomimetic hydrogels, Biomacromolecules **17**, 2642 (2016).
[62] S. Plimpton, Fast parallel algorithms for short-range molecular dynamics, J. Comput. Phys. **117**, 1 (1995).
[63] See Supplemental Material at http://link.aps.org/supplemental/10.1103/PhysRevMaterials.4.085601 for (i) simulation details, (ii) quantification measures, (iii) self-interaction parameters, (iv) radius of gyration, (v) final configurations and their probabilities, and (vi) figures for shape factors in real and Fourier space.
[64] D. N. Theodorou and U. W. Suter, Shape of unperturbed linear polymers: Polypropylene, Macromolecules (Washington, DC, U. S.) **18**, 1206 (1985).
[65] A. Stukowski, Visualization and analysis of atomistic simulation data with OVITO—the open visualization tool, Modell. Simul. Mater. Sci. Eng. **18**, 015012 (2009).
[66] https://github.com/vaidyanathanms/graft_methylcellulose.
[67] http://hdl.handle.net/11299/213785.